NUMERICAL SIMULATION OF ANODIC REACTIONS

Gary E. Giles
Computational Physics & Engineering Div.,
Oak Ridge National Laboratory, Oak Ridge, TN 37831-6415
Leonard J. Gray
Computer Science and Mathematics Div., Oak Ridge National Laboratory, Oak Ridge, TN 37831-6367
Jonathan S. Bullock, IV
Development Div., Oak RidgeY-12 Plant, Oak Ridge, TN 37831-8096
Gary J. Van Berkel
Analytical Sciences Div., Oak Ridge National Laboratory, Oak Ridge, TN 37831-6365

ABSTRACT

Two electrochemical systems have been simulated, with a focus on the anodic reactions and associated phenomena. These systems are the Scanning Reference Electrode Technique instrument scanning an anodically-polarized surface, and an electrospray ion source operated in the positive ion mode. In both of these systems the region of interest is small (10-200 μm). The numerical technique used in the simulation was able to incorporate: features as small as 0.5 μm; multiple reactions at the anode surface; and nonuniform surface properties. Ion transport was modeled by the Laplace equation, together with nonlinear concentration and activation polarization boundary conditions on electroactive surfaces. The Laplace equation was solved using a boundary integral analysis, and the nonlinear polarization equations were satisfied via either a successive-substitution (Picard) or a two-step Gauss-Seidel iterative technique. Successive iterations for the polarization are determined from the previous iteration's current density distribution. This iterative process continued until the change in the boundary potentials was less than a specified tolerance.

INTRODUCTION

The simulations reported in this paper were performed with modified versions of the BEPLATE code(1-3). BEPLATE was originally developed and successfully applied to simulate electroforming on complex three-dimensional mandrels. BEPLATE uses the Boundary Integral technique with boundary conditions to simulate the ion transport and electrochemical kinetics boundary effects. Most of the scenarios that have been successfully analyzed prior to this work were of normal engineering scale (on the order of 1 mm to 1 meter) and involved single, fairly well understood electrochemical processes. In this research, we have modified and applied the technique to simulate detailed electrochemical processes on μm- to mm-scale features. The technique has also been extended to allow simulation of two parallel anodic electrochemical processes, as well as spatially-variable electrochemical parameters. The first system described in this paper is the Scanning Reference Electrode Technique (SRET) instrument (4). The SRET

instrument measures the potential difference between two small pseudo-reference electrodes on a probe scanned over a sample surface. The other electrochemical system is an electrospray (ES) ion source (5). The electrospray system generates gas-phase ions for detection by mass spectrometry. Only a small subset of each of these system were modeled. The regions modeled are shown in Fig. 1a and 1b.

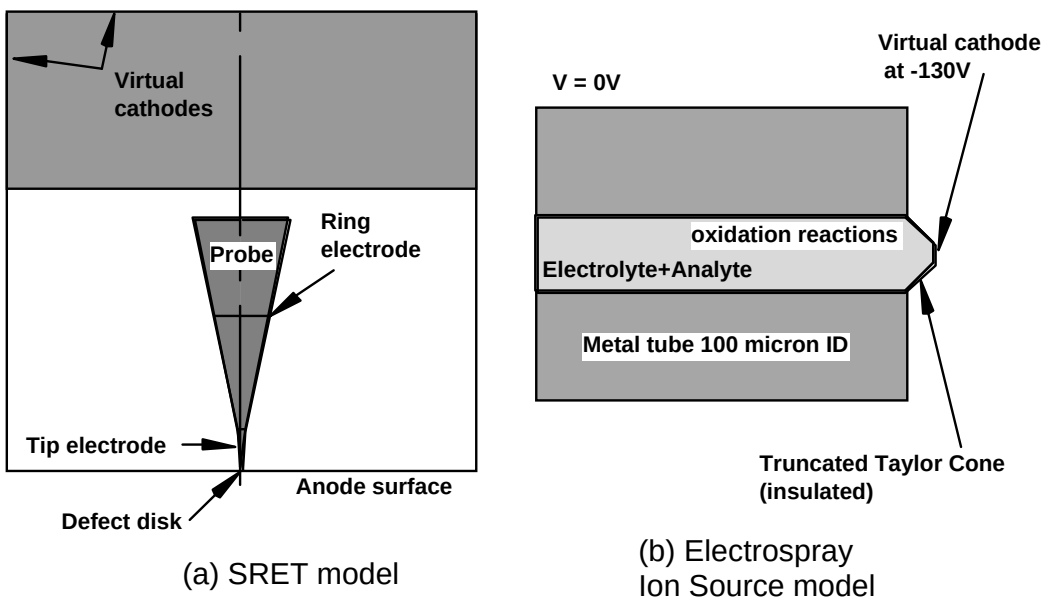

Fig. 1 Two anodic electrochemical systems modeled.

Both simulations focus on the oxidation of chemical species on inert metal anodes. The goals of this work were to better understand the details of the operation of these two devices and to demonstrate the ability to model complex electrochemical systems.

Governing Equations. This model of electrochemical systems assumes that the transport (diffusion, convection, and migration) and reaction of ions can be approximated by solving the Laplace equation for the potential through the electrolyte volume, and then applying a scalar factor representing the electrolyte conductivity, to produce a current density distribution. The scale of these problems is small, but we do assume that continuum conditions apply. The numerical solution must satisfy the nonlinear boundary conditions at the electroactive surfaces (electrodes). These boundary conditions approximate the effects of electrochemical surface reactions (activation polarization) and of mass-transfer effects (concentration polarization). Constant electrical conductivity is assumed throughout the electrolyte, and thus all nonlinearities are on the boundaries.

The oxidation of species at the metal-solution interface is described by Faraday's law. The oxidation rate Ω (equivalents/s-cm^2) is proportional to the current density I (A/cm^2) at the anode surface,

$$\boldsymbol{\Omega} = \frac{\varepsilon}{nF}\,|I|, \tag{1}$$

where F is Faraday's constant, ε is the current efficiency of the process (assumed to be 1.0 in this study), and n is the number of electrons per mole of the reaction. The current density on the anode is in turn proportional to the normal derivative of the potential $\phi(x,y,z)$,

$$I \;=\; \boldsymbol{k}\nabla\phi \cdot \tilde{n} \;\equiv\; \boldsymbol{k}\,\frac{\partial\phi}{\partial\tilde{n}}, \tag{2}$$

where $\tilde{n}$ is the surface (unit) normal vector and $\boldsymbol{k}$ is the conductivity of the electrolyte (Mho/cm). The potential field ϕ satisfies the Laplace equation

$$\nabla^2\boldsymbol{\phi} = 0\,. \tag{3}$$

Thus, the current density is obtained by solving eq 3 subject to specified boundary conditions. The boundary of the region (Σ) consists of: (i) insulated surfaces, for which the applied boundary condition is zero normal flux ($\partial\phi/\partial\tilde{n}$ = 0); and (ii) potential surfaces (anode and cathode). Using Green's Theorem, it can be shown that the Laplace equation is equivalent to the boundary integral equation

$$\phi(P) + \iint_{\Sigma} \frac{\partial G(P,Q)}{\partial\tilde{n}}\,\phi(Q)dQ \;=\; \iint_{\Sigma} G(P,Q)\,\frac{\partial\phi(Q)}{\partial\tilde{n}}\,dQ \tag{4}$$

where the Green's function is the point source potential

$$G(P,Q) \;=\; \frac{1}{4\pi\|P - Q\|}\quad . \tag{5}$$

Here, the gradient and the surface integration are with respect to the boundary point Q, P is an arbitrary point on the boundary Σ, and $\|P - Q\|$ is the distance between P and Q. Eq 4 provides, for each P, a linear relationship between the values of ϕ and the gradient of ϕ on the boundary, and is the starting point for the Boundary Element Method.

The boundary condition on the anode for these equations is not simply the applied potential; it must also take into account the nonlinear transfer (polarization) function describing the physical phenomena occurring in the boundary layer near and at the surface. In the analysis of the systems described in this paper a virtual cathode and also bounding insulated surfaces are used to reduce the model size. The virtual cathode represents a surface of constant potential and completes the circuit of the electrochemical cell. Since the virtual cathode represents an isopotential surface in space, no electrochemical reactions occur on it. Thus, the usual cathode potential components are not applicable and are replaced by a constant V_C.

The polarization functions on the anode specify a nonlinear relationship between the current and the potential difference across this layer, making the entire

problem nonlinear. Specifically, if V_A and V_C denote the applied anode and cathode potentials ($V_A \geq V_C$), the applied potential difference $V = V_A - V_C$ can be decomposed as a potential drop in the electrolyte, ΔV_{ir}, plus interfacial potential drop across the electrolyte boundary layer, made up of the overvoltage η and the associated equilibrium potential values E^0 (Eq. 6). This is schematically illustrated in Fig. 2 for a system involving two anodic reactions.

$$V = (E^0 + \eta_T) + \Delta V_{ir} - V_C \tag{6}$$

In general, the polarization is specified by the solution of the nonlinear relationship between the local current density and the overvoltage,

$$I = F(\eta) \tag{7}$$

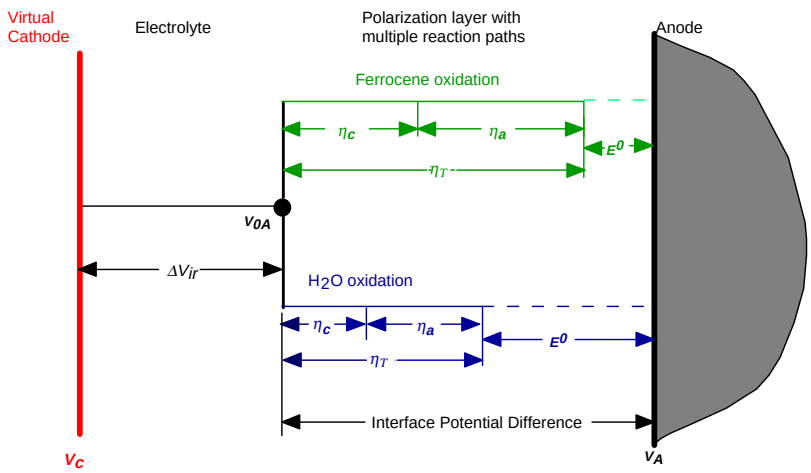

Fig. 2 Schematic of multiple reactions polarization model

The unknown overvoltage, together with the equilibrium potential for each reaction at the anode and the virtual cathode potential, define the electrode boundary conditions for the Laplace equation, and must be determined self-consistently with eqs. 3, 6, and 7. In this work, the total anode overvoltage, η_T is comprised of two components, one part due to the effects of electron transfer (activation polarization η_a), and the other due to the effects of mass transfer (concentration polarization η_c):

$$\eta_T = \eta_a + \eta_c \,. \tag{8}$$

(Other resistance effects at the interface, which would have different transfer functions, are ignored for this analysis.) For activation polarization, the current/potential relationship is given by the modified Butler-Volmer equation,

$$I = I_0 \left(e^{\frac{\alpha_A F}{RT}\eta_a} - e^{-\frac{\alpha_C F}{RT}\eta_C} \right), \tag{9}$$

while the functional form of the concentration polarization is

$$\eta_c = \frac{RT}{nF} \ln(1 - \frac{I}{I_L}) \quad . \qquad \textbf{(10)}$$

In these equations R is the gas constant, T is the temperature in Kelvin, α_A and α_C are the anodic and cathodic transfer coefficients, and I_0 is the exchange current. The α_A, α_C, and I_0 are the parameters that control the activation polarization. I_0 is the value of either anodic or cathodic current (at equilibrium, where these two currents are equal and opposite) associated with zero activation overvoltage ($\eta_a = 0$). Since at zero activation overvoltage the external currents are zero, I_0 must be determined indirectly by extrapolation on a Tafel [log(current) versus potential] plot. The transfer coefficients α_A and α_C are in general different and essentially define, with I_0, the rate constants for the cathodic and anodic reactions at the electrodes. All of these parameters are dependent on the specific electrode reactions, electrolyte composition, etc., and are experimentally determined. All potentials are with respect to the standard hydrogen electrode (SHE) at 0.0 V.

The limiting current density I_L, (which is the maximum value of the rate of transfer of electroactive species to or from the surface across the concentration boundary layer), is the primary variable controlling the concentration polarization.

The concentration (or diffusion) boundary layer is defined as the region near the electrode through which mass transport perpendicular to the electroactive surface occurs only by diffusion. The outer boundary of this layer is determined by the point at which the concentration of the reacting species is equal to the bulk value. This position is generally determined by a linear extrapolation of the near-surface concentration gradient to the bulk concentration. The diffusion layer is thinner than the hydrodynamic (momentum) boundary layer. For an electrochemical reaction that consumes species from the electrolyte, reactions at the surface will decrease the concentration near the surface. The limiting current is reached, for example, when the concentration of a consumed species at the surface approaches zero and reaction current must be entirely supported by the molecules that are diffusing across the concentration boundary layer. The diffusion coefficient will thus limit the amount of the species that can react at the surface per unit time. Mass transfer effects due to the general fluid flow in the electrolyte and streamwise depletion have been ignored in this model.

Polarization Iterative Techniques

In previous work we developed a modified Picard iteration scheme, combined with relaxation and acceleration techniques, to solve the nonlinear polarization equations (1). In this approach, the next guess is a weighted average of the two previous values. This method has been successful, but depending upon the geometry and the system parameters, convergence could be quite slow. The main difficulty with this method is that all values change at every step of the algorithm, which can cause oscillation, and each iteration requires a complete solution and is therefore computationally expensive. This method was applied to the electrospray simulations described below. Successful convergence required very limiting relaxation factors and several hundred thousand iterations.

In the present work, a new iterative algorithm has been developed. This method employs a two-stage process, the inner iteration being a Gauss-Seidel technique in which nodes on the anode are updated individually, requiring very little calculation. When this process has roughly converged, the expensive global solution is then

executed in the outer iteration. Our limited experience indicates that this technique is more robust than the Picard iteration, and converges much faster (about 1 to two orders of magnitude fewer iterations). An additional advantage of this approach is that no guessed-at relaxation or acceleration factors are required. This new method was applied to the SRET simulations, substantially reducing the computational time required.

Polarization Model for Multiple Reactions. There is the possibility of multiple reactions occurring simultaneously at the anode. For the purposes of simplicity in this initial study, all reactions were assumed to be anodic and thus to contribute an algebraically positive portion of the total current, which is the sum of the currents for each reaction. This multiple-reaction modification was applied to the electrospray but not to the SRET model. Multiple reactions were modeled as parallel electrical (ion) paths at the surface with separate activation (eq 9) and concentration (eq 10) polarization and separate equilibrium potentials as shown in Fig. 2.

For a given location, the potential on the electrolyte side of the polarization region, i.e. the interface potential V_{0A} in Fig. 2, is assumed to be the same regardless of the reaction. The equilibrium potential and polarization components for each reaction ($E^0 + \eta_a + \eta_c$) must sum to $V_{0A} - V_A$ at this point. The total current from V_{0A} to V_A is the sum of the currents of the individual reaction components. A solution is found when these conditions are satisfied.

APPLICATIONS

The SRET Instrument

In the SRET instrument, a small probe containing two pseudoreference electrodes is scanned across a surface to detect small changes in the rate of electrochemical processes due to surface reaction or geometric inhomogeneties, Fig. 1a. The mechanical resolution of the instrument can be made to be 1.0 μm in the two horizontal scanning directions (x,y) and 0.5 μm in the vertical direction (z). The vertical probe location above the sample surface while immersed can usually be optically estimated to within 50 μm. For the currently tested situation, a small current between the virtual cathode and the anode establishes an electric field which drives the oxidation of water at the anode surface. The oxidation process modifies the electrical field distribution; this modification is detected by the scanning probe pseudoreference electrodes as a change in the potential difference between the two electrodes. Numerical simulation allows detailed predictions of the effects of the electroactively variable area (defect) size and relative difference in electrochemical properties (contrast). The purpose of this study was to determine limits of detection of typical defects.

The first SRET analysis simulated oxygen generation on the surface of a small (200 μm in diameter) gold disk situated on the surface of an insulating plane. The electrochemical parameters are assumed to be uniform over the disk surface. These simulations were performed on a model of the electrolyte volume within 10,000 μm of the disk. The geometry and potential of the virtual cathode was adjusted to achieve the measured total current on the anode. A ring virtual cathode at the top of the cylindrical

wall produced reasonably uniform current densities over the span of the gold disk and allowed the necessary probe translation with enough clearance to prevent the virtual cathode, probe and insulating boundaries from interfering with each other. The probe was modeled as an insulating volume. The pseudo-reference potentials were determined from points representative of the electrodes on the probe-shaped insulating volume. The shape of the tip electrode and the body of the probe were modeled. The ring electrode was not explicitly modeled. No bi-polar effects or electrical flow paths between electrodes external to the electrolyte were modeled.

These analyses were performed to give confidence in the application of the BEPLATE code to this system. The simulations produced potential difference vs. position profiles qualitatively similar to those observed in experiments. The average potential change produced was 12 mV and the Full-Width-at-Half-Maximum was 400 µm for a calculational experiment with an electrical conductivity of 1.5×10^{-4} S/cm and a probe height of 150 µm. [Other parameters for this analysis were: $\alpha_A = 0.493$, $I_{0A} = 1 \times 10^{-12}$ A/cm^2, $E_{0A} = 1.229$ V vs SHE, $I_L = 5.36$ A/cm^2, $D = 1 \times 10^{-5}$ cm^2/s] Since there was a significant potential gradient from the top and bottom of the probe tip electrode, the average is reported. This compares fairly well with the experimental values of 11.5 mV and XX µm. This model was also used to investigate the effect of scanning probe height, total current and electrochemical parameters. The effect of changing the probe height is much greater than changing the total current and might be used as a means of detecting probe height. The expected possible variation from nominal electrochemical parameters produced only small changes in the potential differences.

Simulations of the full model with a complete sample disk (2.175 cm diam.) indicated that, with the exception of the very edge of the disk, the current density is fairly uniform. Thus, water oxidation occurs fairly uniformly over most of the surface of the sample disk. The small region of elevated current density at the edge was found to not measurably affect the electrical field at the specified probe electrode height. In order to extract the detailed potential difference on the scale of the experiment, a model with much smaller elements was required. Unfortunately, a full model (complete with anode and cathode modeled in detail) would have required more computational resources than available. Also, the larger model would not have conveniently allowed the probe to be accurately scanned across the sample.

A more tractable, detailed model of the electrolyte volume within 5,000 µm of the center of the sample disk was used to analyze a uniform disk of metal with a small region having a different local exchange current. These simulations were preformed on a smaller model than the gold disk simulations. The virtual cathode in this model was changed from the upper portion of the bounding cylinder to be the disk at the top of the modeled cylinder. The current density variation across a 10 µm radius defect is presented in Fig. 3a and 3b. The very rapid change in current density at the edge of the defect was expected and the trends observed (for the differing contrast) are physically reasonable, indicating that the modification to incorporate local electrochemical property differences into the model is effective.

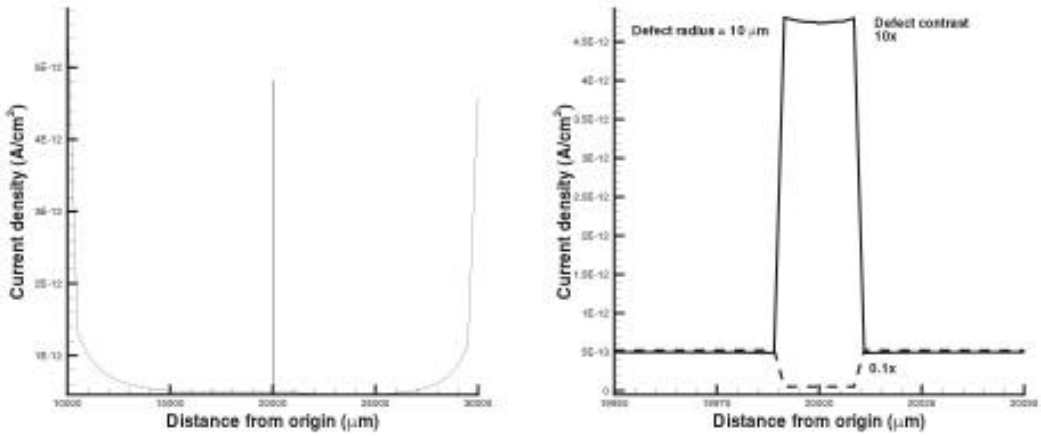

(a) (b)

Fig. 3 Calculated current density through the center of the defect, radius = 10 mm. (a) across disk, (b) detail around defect with differing defect parameters.

The effects of differing defect sizes are compared in Fig. 4. The normalized potential difference for defects of 10 μm radius and differing contrast are presented in Fig. 5. The potential differences have a similar trend as the gold disk analyses and indicate the ability of the instrument to detect this defect size and contrast. (These results were adjusted for grid dependencies, using results from an equivalent case without any defect under the assumption that the grid dependencies will effect the calculations in the same manner. Since the grid are sometimes a significant portion of the signal we are trying to measure in the simulation, these trends must be validated by experimental data when it is available.) The model was also used to investigate probe height variations.

The Electrospray Experiment (5,6)

The ES ion source is used to generate gas-phase ions from analyte species originally in solution, for analysis by mass spectrometry (MS). The ES ion source configuration investigated in this paper, is comprised of two electrodes, e.g.: a narrow bore metal ES capillary or emitter (i.e., the working electrode), held at a high positive potential (positive ion mode) or negative potential (negative ion mode); and the atmospheric sampling aperture plate (i.e., the counter electrode) of the mass spectrometer, held at a potential at or near ground. During typical ES-MS operating conditions, a solution of an analyte is pumped through the ES emitter, and sprayed towards the aperture plate. The applied electric field causes ions of the same polarity as the potential applied to the ES capillary to migrate in the liquid towards the capillary tip. When the buildup of an excess of ions of one polarity at the surface of the liquid reaches the point that coulombic forces in the gap are sufficient to overcome the surface tension of the liquid, droplets enriched in one ion polarity are emitted from the

capillary. This results in a quasi-continuous steady-state current at the counter electrode with a direction consistent with the polarity of the potential difference (7).

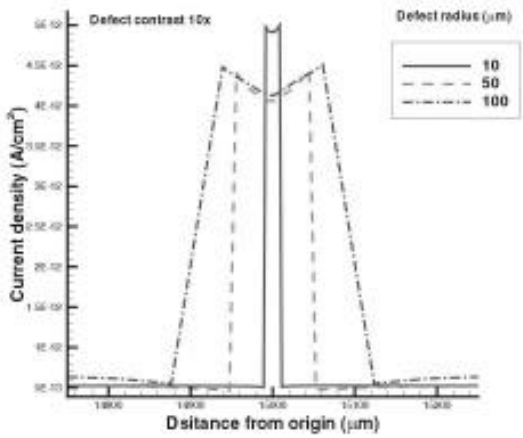

Fig. 4 Current density across different sized defects

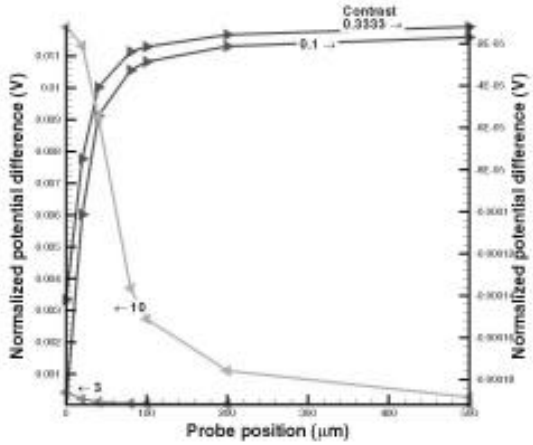

Fig. 5 Normalized potential difference for defects with different parameters.

Charge balance is maintained in this device through electrochemical oxidation/reduction of the components of the metal ES emitter and/or one or more of the species in the solution. Oxidation reactions occur in the ES emitter in positive ion mode, while reduction reactions occur in negative ion mode. The current existing at the emitter owing to these reactions (i.e., the faradaic current) is equal in magnitude but opposite in polarity to the current measured at the counter electrode (i.e., the ES current). The discharge of excess ions and/or creation of ions of the appropriate polarity thereby supports an excess of one ion polarity in the charged droplet. Reduction/oxidation of some species at the counter electrode occurs to complete the electrical circuit.

For the purposes of the investigation of the electrochemical processes, only the electrolyte near the end of the emitter and the Taylor cone at the exit was modeled. The tip of the Taylor cone, which under typical conditions extends to form a jet that then breaks up into droplets, has been truncated and modeled as a virtual cathode.

The Specific ES System Modeled. The model was developed for an ES ion source of the basic geometry with a 100 μm-i.d. inert metal ES emitter held at a positive 3.5 kV relative to a counter electrode at ground, spaced 1.0 cm away. The solvent/electrolyte system was CH_3CN/H_2O (90/10 v/v) containing various concentrations of ferrocene (Fc, dicyclopentadienyl iron). The most prominent redox reactions within the emitter under these conditions were assumed to be H_2O and Fc oxidation.

The products of the redox reactions within the ES emitter travel in the liquid from the inner emitter wall, through the tube, into the Taylor cone, out the jet, and into charged droplets. In our simulation, the locus of current transfer into the jet is modeled as a flat-disk virtual cathode (of fixed potential). The potential difference, *V*, between the emitter (anode) and the virtual cathode was fixed in this BEPLATE code simulation at -130 V. This value, when used in the model, produced the same ES current (i.e., 5.21×10^{-8} A) as that experimentally measured at a solution flow of 5.0 μL/min using the ES geometry and solvent composition described below.

The three solvent systems simulated for the ES system model in this work were: (1) pure CH_3CN with 5.0 μM Fc; (2) CH_3CN/H_2O (90/10 v/v); and (3) CH_3CN/H_2O

(90/10 v/v) containing 5.0 µM Fc. Three different scenarios were modeled: ferrocene oxidation only; water oxidation (i.e., oxygen generation) only; and both ferrocene and water oxidation. The electrical conductivity was 3.8 x 10^{-7} S/cm. The oxygen generation electrochemical parameters were the same as in the SRET simulations. The ferrocene electrochemical parameters were: $\alpha = 0.493$, $I_{0A} = 1 \times 10^{-10}$ A/cm^2, $E_{0A} = 0.572$ V vs. SHE, $I_L = 4.82 \times 10^{-5}$ A/cm^2, $D = 2.4 \times 10^{-5}$ cm^2/s.

The predicted current density (A/cm^2) and interface potential (V_{0A}) for all three systems are compared in Figs. 6a and 6b. The current density distributions for two of the cases (for both reactions, and for oxygen generation only) show large current densities at the tip (at 0 µm) while decreasing rapidly (by 3-4 orders of magnitude) within the first 300 µm into the emitter. The Fc-only curve is flat, indicating that the current density on the anode surface is nearly uniform.

While the Fc-only results are numerically correct they are perhaps not physically meaningful. The constant current density is a consequence of the system being constrained by the low limiting current of the Fc reaction and the limited length of the model (1000 µm). This simulation applied a constant potential difference (130V) across the virtual cathode and the anode. This potential difference was chosen from the two-reaction model results to provide the same total current as the experiment. Unfortunately, for the Fc-only case this large a potential difference drove the nonlinear concentration polarization far from normal values and produced a very large potential difference across the polarization layer. Although this condition is not physically realistic (because other processes would intervene and prevent this large a potential difference from ever being established), this simulation does illustrate what can happen when the limiting current is low enough to cause the whole surface of an anode to be at the limiting current values. Very uniform current density distributions and high potential drops can be obtained. As a consequence of this over-constrained condition, the interface potentials for the Fc-only model are much larger than for the other systems and were omitted from Figure 6b.

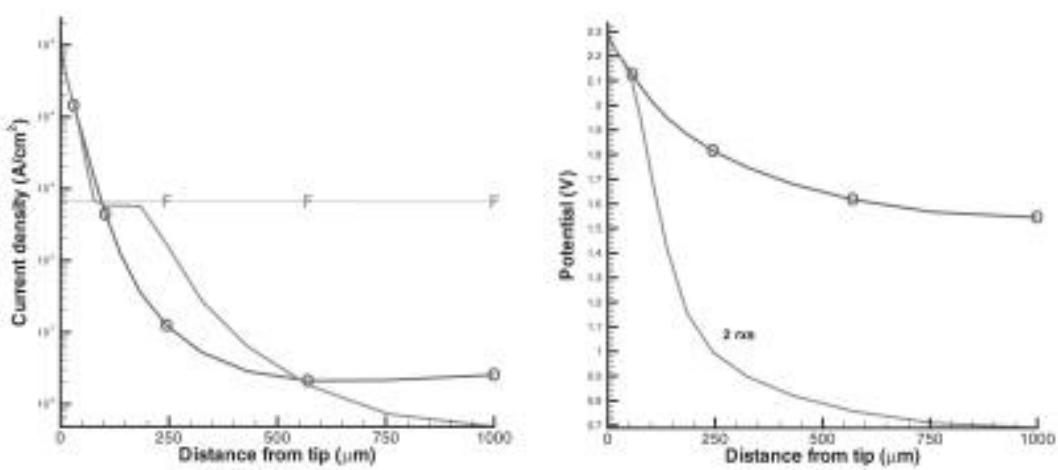

(a) (b)

Fig. 6 Single reaction current density (a) and potential (b) compared with multiple reaction results as a function of distance from the tip of the emitter.

The predicted interface potential distribution (V_{0A}) and the current densities (A/cm^2) for the two-reaction system are shown in Fig. 7 for two models with differing ferrocene oxidation limiting current values. V_{0A} includes the effects of the equilibrium potential and of activation and concentration polarizations for both reactions . The plot in Fig. 7a covers the region from the spray tip of the emitter up to 1000 µm upstream, while the plot in Fig. 7b shows just the 250 µm region at the tip. As one moves from the upstream region of the emitter to the spray tip, the total current density gradually increases, until it goes through a rather complicated transition near the tip. This is due to the relative electrochemical parameters of the two competing, parallel redox processes. In the low current density region, far from the tip, Fc oxidation supplies the majority of the current. As one approaches the tip, the rate of this reaction increases to a point limited by the maximum achievable flux of material to the electrode, i.e., the limiting current, I_l. An increase of V_{0A} beyond this value cannot increase the rate for this reaction. To supply more current, the interfacial potential increases, which increases the rate of H_2O oxidation. Therefore, both the interface potential and current owing to H_2O oxidation are observed to increase substantially at about the same point as which the limiting current for the Fc reaction is reached. The current due to H_2O oxidation continues to increase as one travels downstream. Limiting current changes can be seen to change the potential, current distributions and relative amounts of the two reactions throughout the emitter. Studies of the effects of concentration of the ferrocene and the electrical conductivity of the supporting electrolyte (ACN) are included in Ref. 6. A Tafel plot of this data shows trends that are consistent with the electrochemical parameters.

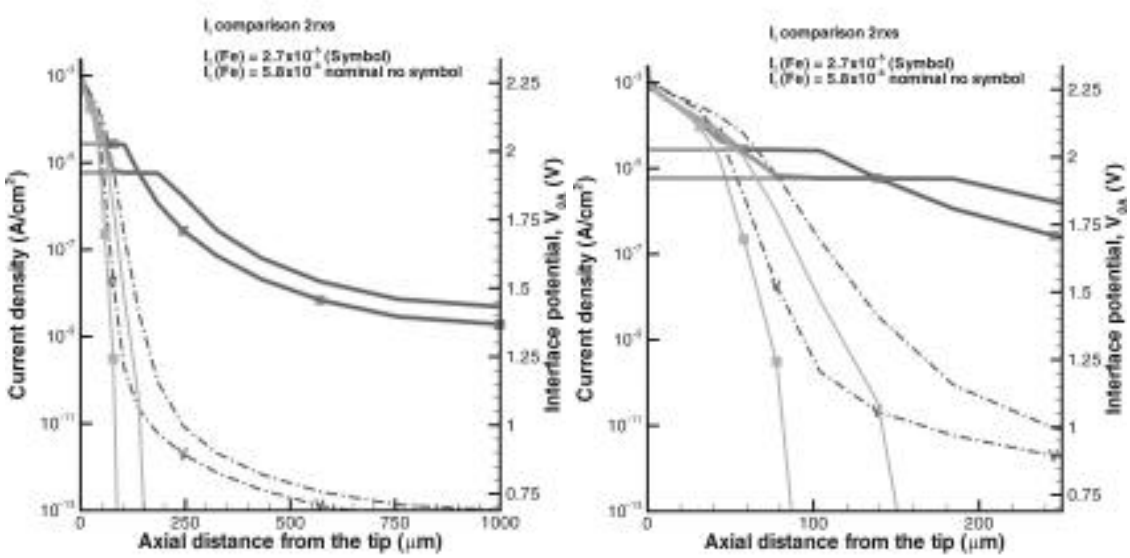

Fig. 7 Current density and interface potential as a function of distance from the tip for cases with different limiting currents for Fc+. (a) complete length of anode, (b) first 250 µm of anode.

SUMMARY

The results presented here represent the computational simulation of the electrochemical operation of two electrochemical systems. This was accomplished through adaptation of the BEPLATE™ code, originally developed for large-scale electroforming simulations. The new features in this work are the small scale of these systems, the ability to use nonuniform polarization parameters, and the multiple, competitive redox reactions in the ES emitter problem. Although the simulations were computationally intensive, converged solutions were achieved. These provided predictions of the either the SRET probe potential difference and sample current density distribution, or the interface potential and the current densities of each reaction for the ES emitter problem. These problems challenge the numerical technique in two different ways. First, the extremely large change in the element size across the span of the SRET probe analysis provided numerical difficulties in producing a solution. Secondly, the non-linear, multiple-reaction polarization equations challenged the iterative process in achieving converged solutions for the ES emitter polarization iterations. These studies were used to optimize an application of the system using the SRET, and to predict the sensitivity of the system prior to experimental studies.

From this initial modeling of these electrolytic systems, several major pieces of information were obtained. For the SRET analysis, a possible technique for determining the probe elevation, that may be due to the shadowing effect of the probe as it is lowered to the surface, was identified. Second, the ability to simulate variations in electrochemical parameters across an otherwise featureless surface, yielding variable current densities, has been demonstrated for the BEPLATE code. For the ES analysis, the computational simulations predicted basically the same electrolytic behavior for the ES ion source as has been observed experimentally and that is consistent with the controlled-current electrolytic cell analogy put forward by Van Berkel and Zhou (8,9). That is, the situation within the ES emitter is not one of controlled-electrode-potential. Instead, the potentials seek those levels required to satisfy the integrated current condition imposed together with the equilibrium potentials and the polarization properties (including both electron-transfer and mass-transfer polarization components) of the one or more redox reactions that can take place. The model predicts actual values of the potentials at the emitter surface as a function of location, as well as the amount of current supplied by each of the different redox reactions.

Also important was the determination of the effective electrode area within the ES emitter. Although the total length of the inner surface of the emitter modeled (1 mm in length) was in contact with the electrolyte, the majority of the current owing to the redox reactions (that may realistically be expected) originated within a 200-300 μm region near the spray tip. This limited effective anode area, equal in length to approximately three emitter inner diameters or less, is a direct consequence of the limited penetration of the electric field into this high-aspect-ratio geometry under "normal" ES conditions where high currents at the tip cause high IR drops. The current density distribution must follow the limitations of this potential gradient distribution.

ACKNOWLEDGEMENTS

Research sponsored by the Division of Chemical Sciences, Office of Basic Energy Sciences, by the Applied Mathematical Sciences Research Program of the

Office of Mathematical, Information, and Computational Sciences, both under contract DE-AC05-96OR22464 with Oak Ridge National Laboratory, managed by Lockheed Martin Energy Research Corporation; and by Defense Programs of the Department of Energy, under contract DE-AC05-84OR21400 with the Oak Ridge Y-12 Plant, managed by Lockheed Martin Energy Systems, Inc.

REFERENCES

1. Giles, G. E.; Gray, L. J.; Bullock, J. S., IV *BEPLATE - Simulation of Electrochemical Plating*, K/CSD/TM-89, Martin Marietta, (1990).
2. Brebbia, J. C.; Telles, F.; Wrobel, L. C. *Boundary Element Techniques*, Springer Verlag, Berlin and New York (1984).
3. L. J. Gray, *A Program for Solving the 3-Dimensional Laplace Equation via the Boundary Element Method*, ORNL/TM-9816, Martin Marietta Energy Systems, Inc., Oak Ridge National Laboratory, Oak Ridge, Tennessee, (1986).
4. Badger, S. J.: Lyon, S. B.; Turgoose, S., "Modeling the Twin Platinum Probe Scanning Electrode Response", J. Electrochem. Soc., **145**, no. 12, 4074 (1998).
5. *Electrospray Ionization Mass Spectrometry*, Cole, R.B., Ed., John Wiley: New York, (1997).
6. Van Berkel, G. J.; Giles, G. E.; Bullock, J. S .; Gray, L. J., "*Computational Simulation of Redox Reaction within a Metal Electrospray Emitter*", Analytical Chemistry, (1999).
7. Charbonnier, F.; Rolando, C.; Saru, F.; Hapiot, P.; and Pinson, J. "Short-Time Observation of an Electrospray Current", in *Rapid Communications in Mass Spectrometry*, **7**, John Wiley & Sons, Ltd, 707 (1993).
8. Van Berkel, G. J.; Zhou, F. *Anal. Chem.*, **67**, 2916 (1995).
9. Van Berkel, G. J. in *Electrospray Ionization Mass Spectrometry*, Cole, R.B., Ed., John Wiley: New York, 65 (1997).